

Point-defect-induced nucleation of the ω phase

H. Dosch,* A. v. Schwerin, and J. Peisl

Sektion Physik der Ludwig-Maximilians-Universität München, D-8000 München 22, Federal Republic of Germany

(Received 6 March 1986)

The coherent, elastic-diffuse neutron scattering from a $\text{NbO}_{0.020}$ and a $\text{NbO}_{0.009}$ single crystal has been determined experimentally in absolute units. We demonstrate that the lattice distortions around one single oxygen impurity give rise to an intensity map which has the same qualitative features as observed in $\text{Zr}_{1-x}\text{Nb}_x$ alloys. Model calculations for the diffuse scattering have been performed within the framework of Kanzaki forces. It is shown that a so-called "3f" force field with one free parameter is able to reproduce the absolute values of the entire observed scattering pattern. The complementary interpretation of the experimental data as short-range-order scattering demands defect-induced ω -phase embryos which have a volume of approximately ten unit cells. A real-space interrelation between the Kanzaki force model and the picture of defect-induced, local domains of ω phase could be achieved by demonstrating that the local, defect-induced lattice distortions which are associated with the proposed Kanzaki force field contain static fluctuations of ω phase. It is shown that the attraction of the second-nearest-neighbor Nb shell around the oxygen atom is directly correlated to the structure of the locally condensed phase.

I. INTRODUCTION

When the metals Zr or Ti are alloyed with higher- Z elements like V, Nb, or Mo, the occurrence of a trigonal phase [ω phase] can be observed. In the most investigated system, $\text{Zr}_{1-x}\text{Nb}_x$, the ω phase is found under a puzzling variety of circumstances.

(i) For $x < 17$ at. % the ω phase is formed during quenching, for $x > 17$ at. % it is formed during annealing of the sample.

(ii) It has been shown by Moss *et al.*¹ that domains of the ω phase even persist in $\text{Zr}_{0.8}\text{Nb}_{0.2}$ after the sample has been heated to the high-temperature, homogeneous bcc phase. Quasistatic ω -type (short-range) ordering has also been discovered in the phonon dispersion curves of $\text{Zr}_{0.92}\text{Nb}_{0.08}$ (Ref. 2) at $T = 965^\circ\text{C}$.

(iii) Wakabayashi³ found that only 5.0 at. % Zr in Nb creates neutron diffuse scattering intensities which exhibit the typical signature of ω -phase domains (see below).

The occurrence of the ω phase in bcc metals and its structure are intimately related to the common instability of bcc structures for lattice strains in the [111] direction, which gives rise to the well-known local minimum in the phonon dispersion curve of the LA[111] phonons.⁴ (This will be discussed in more detail in Sec. II.)

Quasistatic⁵ ω -phase fluctuations are apparently not confined to substitutional alloys: ω -phase-like diffuse neutron scattering intensities from the interstitial alloy NbN_x have also been reported recently,^{6,7} where, surprisingly enough, the trigonal domains appear to remain even at N concentrations as small as 0.15 at. %.⁶ The understanding of those results in the extremely dilute systems requires, as pointed out by Dosch and Peisl,⁷ the consideration of ω -phase fluctuations that are nucleated around one individual point defect. It is interesting to note at this point that indications of ω -phase-like lattice distortions have also been seen in NbO_x (Ref. 8) (an inter-

stitial alloy which is related to the system NbN_x), whereas the search for ω -phase domains coupled to the lattice distortions around hydrogen in bcc metals ended in a negative result.⁹ Since all the interstitial defects N, O, and H expand the host lattice, the presence of local lattice dilatation strains is obviously necessary but not sufficient to create ω -phase fluctuations in bcc lattices. The defect location and details in the interaction between the impurity and the host lattice atoms seem to be important. It is one of the aims of this study to shed light on this problem.

In the following we present a diffuse neutron scattering study from the system NbO_x for small oxygen concentrations. We demonstrate by presenting a detailed absolute intensity map of the coherent (quasi-) elastic-diffuse scattering that single oxygen impurities in Nb are nuclei for the formation of the ω phase. The obtained results, which show the unambiguous signature of the ω phase, are discussed in reciprocal as well as in real space from two different points of view.

(i) Within the formalism of defect-induced, static lattice distortions, which will be shown to provide an accurate quantitative description of the experimental findings.

(ii) Within the framework of short-range-order diffuse scattering, which allows conclusions on the extension of the ω -phase domains.

We show that both interpretations are correlated in an interesting and instructive way that yields the identification of those lattice distortions which contribute to the local ω -phase condensation.

II. THE ω -PHASE STRUCTURE

For a detailed discussion of the features of the ω phase, the reader is referred to the articles by Hickman¹⁰ and Currat and Pynn.¹¹ The first reports on the structure of

the phase stem from Bagaryatskiy *et al.*¹² and Silcox *et al.*¹³ followed by other somewhat contradictory publications.¹⁴ The finally accepted version of the formation of the ω phase is illustrated in Fig. 1, which shows the bcc unit cell with three equidistant (111) planes. When the ω phase is created, two neighboring (111) planes move towards each other by a displacement \mathbf{u}_{111} in the [111] direction, while each third (111) plane remains unmoved. The fully collapsed ω phase is described by a displacement $\mathbf{u}^* = \pm(a_0\sqrt{3}/12)(1,1,1)$ and gives rise to superlattice reflections¹⁵ at $\mathbf{G}_{sl} = \mathbf{G}_{hkl} + \mathbf{q}_{bcc}$, where $\mathbf{q}_{bcc} = \frac{2}{3}(1,1,1)$ is the momentum transfer associated with the minimum in the LA phonon dispersion relation. Note that the (quasi)static modulation of the (111) planes, as shown in Fig. 1, can be formally described by a "frozen" LA phonon with a wave vector \mathbf{q}_{bcc} . If the displacement $|\mathbf{u}_{111}|$ is less than $|\mathbf{u}^*|$, then the structure is called the "rumped" ω phase,¹² and elastic-diffuse scattering around the superlattice points \mathbf{G}_{sl} is found, as demonstrated by Moss *et al.*,¹ for the alloy $Zr_{0.8}Nb_{0.2}$. Figure 2(a) shows a part of their observed intensity map which is attributed to the presence of ω -phase domains embedded in the bcc matrix. Pynn¹⁶ presented a one-dimensional model for a qualitative description of the intensity pattern. Borie *et al.*¹⁷ could describe the diffuse intensities observed in $Zr_{0.8}Nb_{0.2}$ by a stacking fault model which assumes the crystal to be completely transformed into ω -phase domains (i.e., containing no bcc phase and, accordingly, no fundamental Bragg reflections from the bcc phase). The obvious lack of this elaborate theoretical study is that it cannot account for the real situation of trigonal ω phases which are coherent-

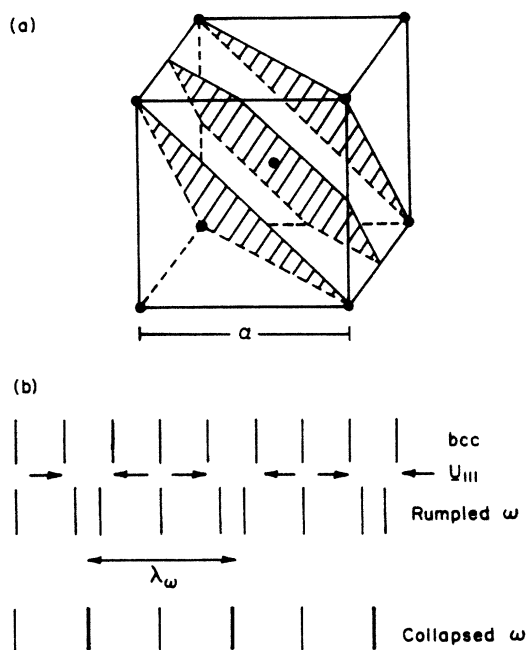


FIG. 1. Formation of the ω phase (see Ref. 11): (a) bcc unit cell with three adjacent (111) planes shaded. (b) Modulation of the (111) planes in the case of the rumped and the collapsed ω phase. λ_ω is the wavelength associated with the ω phase. For u_{111} , see text.

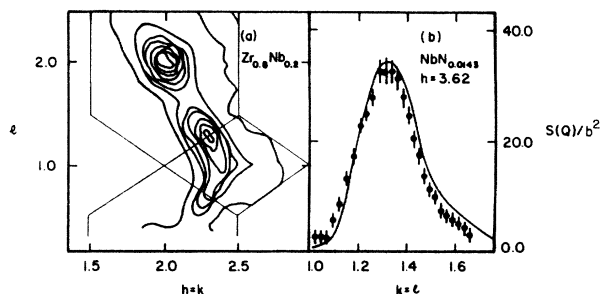


FIG. 2. (a) Part of the iso-intensity map as obtained in $Zr_{0.8}Nb_{0.2}$ (Ref. 1). (b) Elastic-diffuse neutron scattering intensity found in the (233) Brillouin zone of $NbN_{0.0143}$ (Ref. 7): (●) experimental results in absolute units of $S(Q)/b^2$ [Eq. (2)]; (—) model calculation using the Kanzaki forces as given in Table I.

ly embedded in the bcc matrix. A possible key to the development of a model for a partially transformed crystal and for the understanding of the associated diffuse intensities has, as already mentioned before, been found in the dilute system NbN_x . Rowe and Magerl⁶ and Dosch and Peisl⁷ have pointed out that even a small amount of N dissolved in Nb generates diffuse intensity structures which could be related to those obtained in $Zr_{0.8}Nb_{0.2}$ [Fig. 2(b)]. The analysis of the diffuse scattering profiles revealed that they originate from the local lattice distortions around *single* N impurities.⁷ A lattice distortion model has been proposed⁷ within the Kanzaki force formalism¹⁸ (see Table I) which could describe all their experimental results quantitatively [Fig. 2(b)]. Three important questions remained somewhat unanswered.

- (i) Do the diffuse peaks observed in NbN_x [Fig. 2(b)] or NbO_x belong to the same qualitative intensity distribution as found for $Zr_{1-x}Nb_x$ [Fig. 2(a)]?
- (ii) Can this entire scattering distribution be described quantitatively by a single lattice distortion model (Kanzaki forces)?
- (iii) How are the host lattice distortions around the interstitial nitrogen (or oxygen) atoms interrelated to local domains of the ω phase?

TABLE I. Kanzaki forces f_i ($i=1,2,3$) and lattice distortions u_{ij} ($j=1,2,3,4$) proposed for O in Nb. The right column shows the results obtained for N in Nb (Refs. 7 and 22).

	O in Nb	N in Nb
Kanzaki forces ($eV \text{ \AA}^{-1}$)	$f_1=2.80$ $f_2=-0.27$ $f_3=0.54$	$f_1=3.00$ $f_2=-0.92$ $f_3=0.50$
Lattice distortions (\AA)	$u_1=0.42$ $u_2=-0.13$ $u_3=0.06$ $u_4=0.07$	$u_1=0.50$ $u_2=-0.20$ $u_3=0.08$ $u_4=0.09$

These points will be discussed in this study for the system NbO_x . We note here, however, that due to the established similarity between the systems NbN_x , NbO_x , TaN_x , and TaO_x , a similar analysis should be applicable for all these interstitial alloys.

III. DIFFUSE SCATTERING FROM NbO_x

Three Nb samples of equal shape [cylinders with 50 mm length and 10 mm diameter, cylinder axis=(110) direction] have been prepared and purified by a 36-h UHV annealing at $T=2425$ K. All three samples exhibited afterwards virtually the same mosaic spread of 0.18° . Then, two of the Nb single crystals were loaded with 2.0 at. % (c_1) and 0.9 at. % (c_2) oxygen, respectively. In order to avoid extensive oxygen precipitations, the samples were exposed to O_2 atmosphere at a temperature of $T=2100$ K, where, according to the phase diagram of NbO_x , the O defects are dissolved as single, randomly distributed point defects.¹⁹ By a rapid cooling of the samples in a He-gas stream, the random defect distribution could be quenched to room temperature.

We have measured the coherent (quasi-) elastic-diffuse neutron scattering from $\text{NbO}_{0.020}$ in those regions in reciprocal space, where, as reported by Moss *et al.* [Fig. 2(a)], the diffuse intensity from ω -phase domain is expected. In the case of N in Nb the structure factor of the scattering process under consideration depends upon the symmetry and the order of the Brillouin zone (BZ).⁷ Whereas virtually zero intensity is found in the (200) Brillouin zone, strong defect-induced scattering is observed in the (211) Brillouin zone⁶ and the (233) and (411) Brillouin zones.⁷ Thus, the experiments have been performed in the (233) and (411) Brillouin zones (Fig. 3), each region being covered with a grid of about 150 points in the form of linear scans in reciprocal space (Table II). For a test of the concentration dependence of the diffuse intensities, one scan in each Brillouin zone (marked with an * in Table II and Fig. 3) was also measured with the $\text{NbN}_{0.009}$ sample.

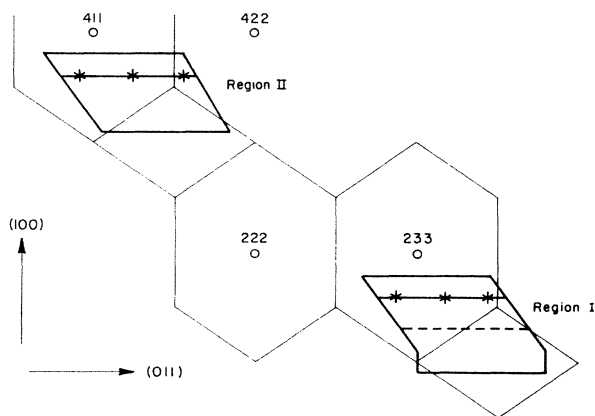


FIG. 3. Measuring program (regions I and II) in the (100)-(011) plane of the reciprocal space. The scans marked with * have been measured for two different oxygen concentrations [see also Fig. 4(a)]. The dashed line in region II indicates the scan shown in Fig. 4(b).

The neutron scattering experiments have been carried out on the triple-axis spectrometer of the Melusine reactor (Centre d'Etudes Nucléaires de Grenoble). In order to reject all strong inelastic scattering processes, the spectrometer was run in an elastic mode with an incident wave vector $k_i = 5.4 \text{ \AA}^{-1}$ [reflected from a Cu(111) monochromator] and a 60'-30'-30'-30' collimation. The neutrons, which were scattered from the sample without energy change, were singled out by a pyrolytic graphite (002) analyzer crystal. The diffuse scattering background from the sample (mainly consisting of incoherent scattering from the Nb atoms²⁰ and, close to Bragg reflections, of weak inelastic scattering) was subtracted experimentally by measuring the corresponding intensities of a pure Nb reference crystal. In Fig. 4(a) we show a typical set of raw data as obtained along a scan in the (411) Brillouin zone (region II). (The counting rates have been calibrated to the effective primary intensity intercepted by the sample.) Note that both oxygen-loaded Nb crystals exhibit a distinct diffuse scattering peak which has a similar shape, as measured in NbN_x [Fig. 2(b)]. The intensity ratio of the two peak maxima is found to be 1.94 and is, thus, not simply given by the ratio c_1/c_2 of the corresponding defect concentrations ($c_1/c_2 = 2.23$). Assuming that the observed intensities stem from a random defect distribution, the underlying coherent scattering cross section $d\sigma/d\Omega(\mathbf{Q})$ has to be written as being proportional to $c(1-c)$ (c =defect concentration) and the so-called static Debye-Waller factor (SDWF) e^{-2L} (note that each coherent scattering is affected by the SDWF^{21,22}):

$$\frac{d\sigma(\mathbf{Q})}{d\Omega} = c(1-c)e^{-2L}S(\mathbf{Q}), \quad (1)$$

where $S(\mathbf{Q})$ is the scattering cross section attributed to one single defect and will be discussed below. Although the SDWF associated with O in Nb has not been measured in detail, it can be related to the experimental values found in the system NbN_x , where the values $2L(400) = 10.5c$ and $2L(011) = 2.5c$ have been measured

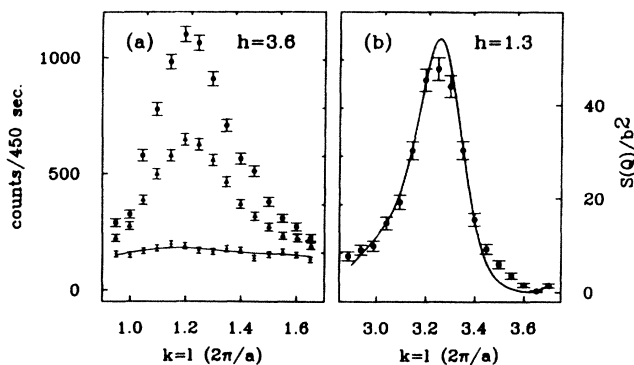


FIG. 4. (a) Raw data obtained along the scan 3.6 0.95*—3.6 1.65 1.65* (Table II): (●) $c_1 = 2.0$ at. % O; (▲) $c_2 = 0.9$ at. % O; (+) pure Nb; the solid line represents a cubic spline fit. (b) Absolute comparison of the final experimental results with model calculations for the 3f model (Table I) along scan 1.3 2.9 2.9—1.3 3.7 3.7 (Table II). Note that the quantity $S(\mathbf{Q})/b^2$ is dimensionless.

TABLE II. Measuring program for the sample $\text{NbN}_{0.020}$ in reciprocal space. \mathbf{Q}_{init} and $\mathbf{Q}_{\text{final}}$ define the end points of the linear scans consisting of 17 equidistant points, respectively (units $2\pi/a$). The scans marked by * (15 points each) have been performed for both oxygen concentrations.

Region I: (233) BZ						Region II: (411) BZ					
\mathbf{Q}_{init}			$\mathbf{Q}_{\text{final}}$			\mathbf{Q}_{init}			$\mathbf{Q}_{\text{final}}$		
1.8	2.65	2.65	1.8	3.45	3.45	3.8	0.70	0.70	3.8	1.50	1.50
1.7	2.70	2.70	1.7	3.50	3.50	3.7	0.75	0.75	3.7	1.55	1.55
1.6	2.75	2.75	1.6	3.55	3.55	3.6	0.80	0.80	3.6	1.60	1.60
1.5	2.80	2.80	1.5	3.60	3.60	3.5	0.85	0.85	3.5	1.65	1.65
1.4	2.85	2.85	1.4	3.65	3.65	3.4	0.90	0.90	3.4	1.70	1.70
1.3	2.90	2.90	1.3	3.70	3.70	3.3	0.95	0.95	3.3	1.75	1.75
1.2	2.95	2.95	1.2	3.75	3.75	3.2	1.00	1.00	3.2	1.80	1.80
1.1	3.00	3.00	1.1	3.80	3.80	3.1	1.05	1.05	3.1	1.85	1.85
1.0	3.00	3.00	1.0	3.80	3.80						
0.9	3.00	3.00	0.9	3.80	3.80	3.6	0.95	0.95*	3.6	1.65	1.65*
1.6	2.80	2.80*	1.6	3.50	3.50*						

for the (400) and (011) Brillouin zones, respectively.²² Since the local distortions around N and O in Nb are quite similar (see below), we estimate the SDWF of O in Nb in the (411) Brillouin zone to be approximately the linear combination of $2L(400)$ and $2L(011)$ and get $2L(411)=13.0c$. Inserting this into Eq. (1), the intensity ratio of the diffuse peaks of Fig. 4(a) is expected to be 1.926, which is virtually observed. Thus, the observed concentration dependence is consistent with the assumptions underlying Eq. (1) and confirms that, in both samples, the oxygen defects were essentially randomly distributed. We discuss in what follows the quantity $S(\mathbf{Q})$ in absolute units. The conversion of the data into an absolute scale has been performed with an accuracy of about 5% through experimentally determined intensities of some host lattice (Nb) transversal-acoustic phonons (which have a well-known structure factor).²³

The absolute scale iso-intensity plot of the observed $S(\mathbf{Q})/b^2$ are shown in Figs. 5(a) and 5(c). In both Brillouin zones we find a diffuse scattering distribution which indeed has the same qualitative features as the scattering pattern found for $\text{Zr}_{0.8}\text{Nb}_{0.2}$ [Fig. 2(a)]. (The theoretical plots in Figs. 5(b) and 5(d) are explained below.) We conclude from this that the oxygen impurity induces local domains of ω phase into the bcc matrix.

IV. DISCUSSION: KANZAKI FORCES AND THE ω PHASE

Regardless of the fact that the observed scattering exhibits the signature of the ω phase, it can be ascribed, in a more general sense, to the local lattice deformations around the interstitial oxygen atom. Thus, the appropriate coherent scattering cross section $S(\mathbf{Q})$ of Eq. (1) has to have the form

$$S(\mathbf{Q}) = \left\langle \left| b \sum_m e^{i\mathbf{Q}\cdot(\mathbf{R}^m + \mathbf{u}_p^m)} + b_D e^{i\mathbf{Q}\cdot\mathbf{R}_p} \right|_p^2 \right\rangle, \quad (2)$$

where \mathbf{u}_p^m is the static displacement of the host lattice atom at site \mathbf{R}^m (with scattering length b) due to the action of a defect located at \mathbf{R}_p . The summation \sum_m has to be performed over the entire long-ranging displacement

field around the defect, giving the so-called “displacement field” amplitude $A_D(\mathbf{Q})$. Since the O impurity shows a nonzero coherent scattering length b_D , the “Laue” amplitude $A_L(\mathbf{Q}) = b_D \exp(i\mathbf{Q}\cdot\mathbf{R}_p)$ has to be taken into account. The diffuse intensity is finally obtained as the square of $|A_D + A_L|$ averaged over all possible defect sites \mathbf{R}_p , denoted by $\langle \rangle_p$. Note that, as a consequence of the assumed random defect distribution, the intensity $|A_D + A_L|^2$ is ruled by the lattice deformation \mathbf{u}_p^m around one individual defect at \mathbf{R}_p . The calculation of $A_D(\mathbf{Q})$ can be carried out by the introduction of Kanzaki forces \mathbf{f}_p^n (applied at the host lattice atoms n around the occupied defect site \mathbf{R}_p) which are related to the lattice deformations \mathbf{u}_p^m through the lattice Green’s function G_{ij}^{m-n} (i, j are the Cartesian coordinates):

$$(\mathbf{u}_p^m)_i = \sum_{n,j} G_{ij}^{m-n}(\mathbf{f}_p^n)_j. \quad (3)$$

Quantitative values for G_{ij}^{m-n} of Nb (Ref. 24) are found via a Born–von Karman fit to the Nb phonon dispersion curves. The obvious advantage of this parametrization of the long-ranging displacement field lies in the appreciable reduction of free parameters, since the Kanzaki forces are confined to the local-defect neighborhood and are supposed to have only radial components. Thus, the forces applied at each neighbor shell around the point defect are completely described by one single number [“force strength,” dimension (eV \AA^{-1})] and so is, through Eq. (3), the entire long-ranging lattice deformation. For a detailed discussion of the calculation of $A_D(\mathbf{Q})$ within this formalism, we refer the reader to the works by Krivoglaз,²¹ Trinkaуs,²⁵ and Dederichs.²⁶

Oxygen (as well as N) is assumed to occupy the octahedral sites²⁷ in the bcc lattice Nb (Fig. 6). Possible sets of forces can be found from the measured dipole moment

$$(\mathbf{P}_p)_{ij} = \sum_n R_i^n(\mathbf{f}_p^n)_j, \quad (4)$$

which has been determined experimentally by Huang diffuse scattering of x rays.²⁸

$$P_{ij} = \begin{pmatrix} 12.4 & 0 & 0 \\ 0 & 5.1 & 0 \\ 0 & 0 & 5.1 \end{pmatrix} \text{ eV.} \quad (5)$$

It has been demonstrated in the case of N in Nb that one needs radial forces which are extended to the third-nearest

$$P_{ij} = \begin{pmatrix} f_1 + 4f_3/\sqrt{5} & 0 & 0 \\ 0 & f_2\sqrt{2} + 8f_3/\sqrt{5} & 0 \\ 0 & 0 & f_2\sqrt{2} + 8f_3/\sqrt{5} \end{pmatrix} a_0, \quad (6)$$

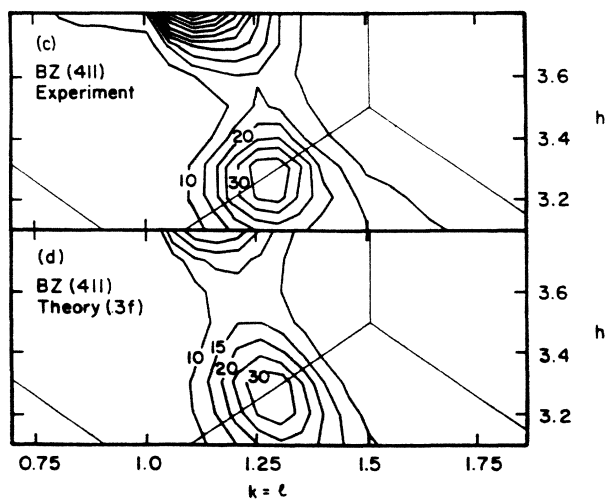
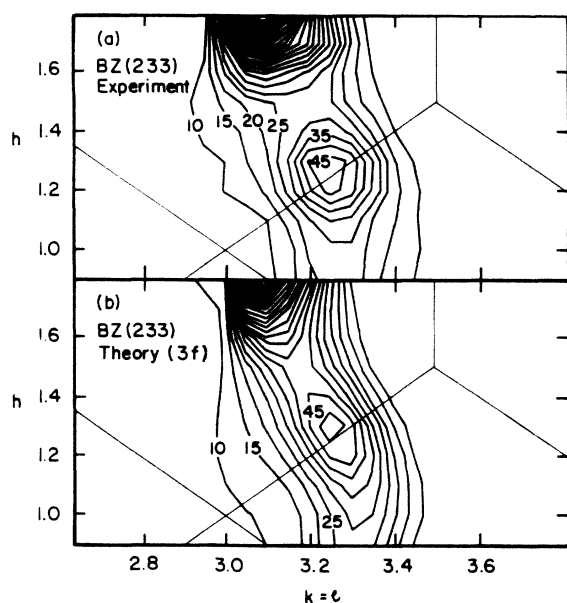


FIG. 5. Absolute iso-intensity plot of the quantity $S(Q)/b^2$: (a) and (c) Experimental results for the (233) and (411) BZ. (b) and (d) Calculated according to the 3f model (Table I) for the (233) and (411) BZ. The lowest levels in each plot is characterized by $S_{\min}/b^2 = 10.0$. The level distance is chosen to be $\Delta S/b^2 = 5.0$.

Nb neighbor ("3f model," see Table I) in order to explain the diffuse scattering intensities as observed along the scan which is shown in Fig. 2(b). It turned out that this concept is also able to describe all our experimental data *quantitatively*. Assuming octahedral site occupancy for O in Nb and radial Kanzaki forces up to the third Nb shell around the oxygen atom, the dipole tensor takes the form

where $a_0 = 3.3 \text{ \AA}$ is the lattice constant of Nb. Thus, two independent linear equations for the three forces f_1 , f_2 , and f_3 follow from Eqs. (5) and (6):

$$f_1 + f_3 4\sqrt{5}/5 = 3.76 \text{ eV \AA}^{-1}, \quad (7a)$$

$$f_2\sqrt{2} + f_3 8\sqrt{5}/5 = 1.55 \text{ eV \AA}^{-1}. \quad (7b)$$

One force remains as a free parameter in the model calculations. Table I shows the set of forces which has been found to provide the best fit to the experimental data. The diffuse intensity patterns arising from this Kanzaki model have been calculated using Eqs. (2) and (3) and are shown in Figs. 5(b) and 5(d). We find that the theoretical results are in excellent *absolute* conformity with the experiment. Note that the experimental and theoretical iso-intensity lines are given in absolute units [of the dimensionless quantity $S(Q)/b^2$]. The remarkable quantitative agreement between the calculated and observed absolute diffuse scattering is also demonstrated in Fig. 4(b) along a typical scan. This allows the unambiguous conclusion that the local distortions u^m which are parametrized by the presented 3f model are the origin of the observed diffuse intensities. (We mention here that, as a by-product of this analysis, the octahedral site occupancy of the interstitial oxygen is proven true.) The distortions $u_{1,2,3,4}$ of the first four Nb shells around the O impurity [calculated via

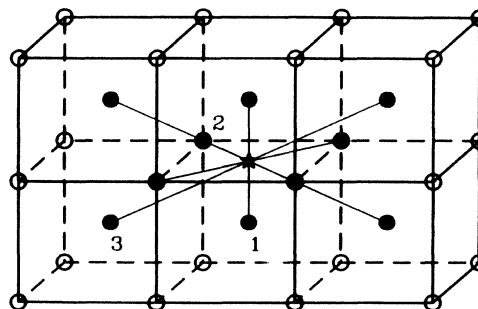


FIG. 6. Defect location of O in Nb [octahedral sites (*)] and Kanzaki forces around one occupied octahedral site on the first- (1), second- (2), and third- (3) nearest-Nb-neighbor atoms. Note that only four (out of eight) third-nearest-Nb neighbors are shown.

Eq. (3)] are shown in Table I and compared to the distortions found around N in Nb.^{7,29} The common features of both local distortion structures are a strong repulsion of the first Nb shell (u_1) and an attraction of the second-nearest Nb neighbors (u_2), followed by an outwards displacement of the third shell (u_3).

We show in the following by employing two complementary interpretations that these heavy local distortions contain the domains ("embryos") of the ω phase.

(i) " $Rq = 1$ " rule. Since the observed scattering exhibits the signature of short-range-order (SRO) scattering, the following analysis of the experimental results is possible:³⁰ the size of the domains can be related to the halfwidth of the observed diffuse peaks around the $\frac{2}{3}(1,1,1)$ positions. This is illustrated in Fig. 7 for the diffuse peak in the (411) Brillouin zone: The circle with radius $q^* = 0.165(2\pi/a)$ confines the region where the diffuse intensity has decreased to $I_{\max}/2$. By the common rule of thumb, $Rq^* = 1$, the reciprocal length q^* , is usually related to a length scale R which characterizes the associated domains in real space. Taking the above value q^* we find $R = 3.2$ Å. If the phase embryos are assumed in a first approximation as spherical regions (with radius R) around the defect, then the associated SRO intensity decays according to the form factor of the sphere as³¹

$$I(q) = I_{\max} \left[\frac{3}{(qR)^3} [\sin(qR) - qR \cos(qR)] \right]^2, \quad (8)$$

with distance q from the intensity maximum I_{\max} . A numerical calculation shows that the condition $I(q^*) = I_{\max}/2$ is then fulfilled for $Rq^* = 1.8148$ or (inserting q^* from above) for $R = 5.8$ Å. This means that the fluctuations of the ω phase must already be established within $R = 3.2$ to 5.8 Å, thus, within a small volume ΔV_{ω} of only a few (approximately ten or less) unit cells. This result proves the recently expressed conjecture⁷ that the ω -phase condensation around the single defects N and O must be

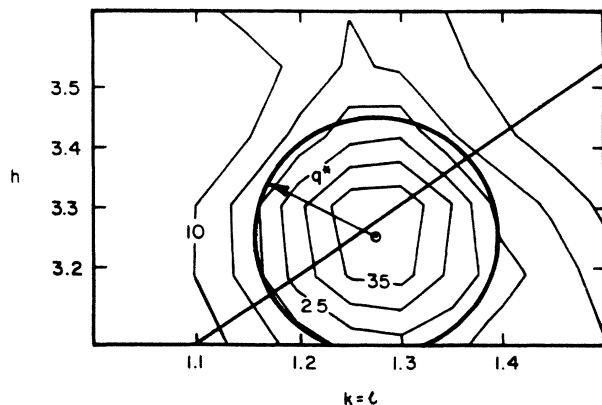


FIG. 7. Estimation of the ω domain size in the (411) BZ. The part of the experimental results in the neighborhood of $\mathbf{q}_{\text{bcc}} = \frac{2}{3}(1,1,1)$ is shown. The circle with radius q^* confines the region where the diffuse intensity has decreased to $I_{\max}/2$ (see text).

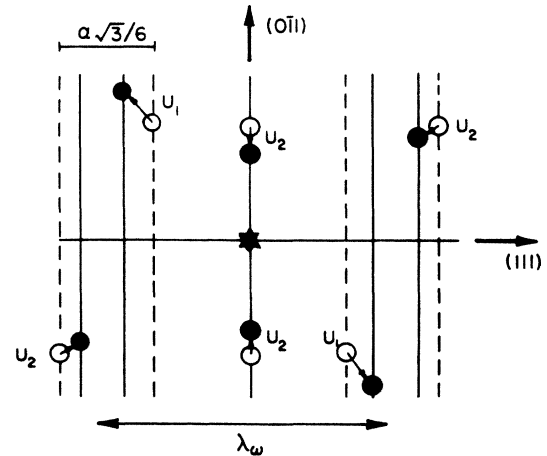


FIG. 8. Location of the Nb atoms of the first and second shell around the oxygen impurity (*) as plotted in the (111)-(0 $\bar{1}$ 1) plane. The open symbols (O) show the Nb atoms in the undisturbed lattice, the solid symbols (●), after introduction of the defect-induced lattice distortions u_1 and u_2 (Table I). The dashed vertical lines denote the (111) planes in the undisturbed lattice ("bcc phase"), the solid vertical lines denote the same planes in the presence of the static displacements of the Nb atoms ("rumpled ω phase"). Note that the (111)-plane distance and the lattice distortions are *not* to scale.

searched for within the strongly distorted defect neighborhood.

(ii) (111) projection of $u_{1,2}$. Consider Fig. 8, which shows the positions of the defect and the host lattice atoms of the first- and second-neighbor shells projected into the plane which contains the (111) direction (the direction where the fluctuation is expected) and the (orthogonal) (0 $\bar{1}$ 1) direction. (The defect site \mathbf{R}_p is chosen as the origin of the coordinate system.) In the undisturbed bcc lattice we get, of course, equidistant (111) planes (dashed lines) which contain all the atoms under consideration (open symbols). The closed symbols and solid vertical lines show the position of the atoms and the (111) planes after the defect (oxygen or nitrogen) and the associated lattice distortions have been introduced: The occurrence of a rumpled ω phase around the defect is clearly visible. We note that the inwardly directed displacement of the second shell ($u_2 = -0.122$ Å for O in Nb and $u_2 = -0.20$ Å for N in Nb) is indispensable to the creation of two pairs of (111) planes that are moved towards each other, separated by an unmoved (111) plane (which contains the defect and two second-nearest Nb neighbors). Since the minus sign of u_2 originates exclusively from the negative radial force f_2 of the $3f$ model, this force should be looked upon as the ω -phase generating part of the defect-lattice interaction and, thus, as the (heretofore missing) connecting link between the Kanzaki forces and static ω -phase fluctuations.

V. CONCLUSIONS

In our final conclusion we want to stress in the following the simplicity of our model compared to other models

in the literature.

(i) The stacking fault model by Borie *et al.*¹⁷ introduces a sophisticated study of the stacking sequence of ω domains in a completely transformed crystal. It is an inherent problem of this elaborate model, as mentioned before, that it cannot account for the presence of the β phase (bcc phase) and for the so-called ω - β interface (transition region between the ω domain and the bcc matrix).

(ii) Recently, Walker³² presented a particle model in order to describe the intensities and halfwidths of ω -phase peaks obtained from an x-ray study on a $\text{Ti}_{1-x}\text{V}_x$ single crystal. The analysis shows that one needs seven free parameters for a satisfactory description of the experimental findings.

The model presented in this work uses only one free parameter and is able to account for all occurring intensities associated with the locally formed ω -phase domains. Our analysis shows that point defects, like N and O, induce local distortions into the bcc metal Nb that contain domains of ω -phase fluctuations. They are coherently embedded in the bcc matrix through a long-ranging static displacement field which itself gives rise to Huang diffuse scattering (HDS) around Bragg reflections. Thus, the ω - β interface and the β phase are included in this model in a natural way. HDS is proportional to the elements of the dipole moment P_{ij} of the Kanzaki forces and, thus, exhibits the tetrahedral symmetry of the defect site (octahedral site). It may appear to the reader at this point as if the observed tetrahedral symmetry of the long-ranged part of the displacement field were somewhat in contradiction to the trigonal symmetry of the locally formed, rumpled ω -phase domains. This seeming inconsistency, however, disappears by a careful differentiation between the internal forces exerted by the defect and the elastic response of the lattice. It is the product of both which determines the

symmetry of the observed lattice deformations [see Eq. (3)]. The Kanzaki forces which determine the entire displacement field around the defect preserve the tetrahedral symmetry of the defect location. The elastic response function of the bcc transition metals exhibits the characteristic instability for (dynamic and static) atomic displacements associated with a wave vector $\mathbf{q}_{\text{bcc}} = \frac{2}{3}(1,1,1)$. Elastic internal forces that have the structure of the presented Kanzaki force field are able to couple to this "local softness" of the matrix and induce noticeable components of the ω phase. It is important to see, however, that the frozen LA(111) phonon shown in Fig. 8 is only *one* (but a strong) component in a Fourier decomposition of the local lattice distortions. Another point must be addressed: In this study we have frequently referred to the similarities of the elastic-diffuse scattering from NbO_x (NbN_x) and $\text{Zr}_{1-x}\text{Nb}_x$ and concluded that similar static fluctuations of the ω phase occur in both systems. However, this does not necessarily imply that the mechanism driving the ω -phase formation is the same in these systems. Since in the case of the substitutional alloys, like $\text{Zr}_{1-x}\text{Nb}_x$ or $\text{Ti}_{1-x}\text{V}_x$, the alloyed atoms have almost the same size, it is most likely that changes in the electronic state rather than the volume mismatch around one individual atom (as discussed in this work) are the origin of the ω -phase transformation there.

ACKNOWLEDGMENTS

We are indebted to B. Renker and J. B. Suck who kindly made the Melousine triple-axis spectrometer available to us and assisted during the experiment. Many stimulating and clarifying discussions with S. C. Moss are gratefully acknowledged.

*Present address: School of Applied and Engineering Physics, Cornell University, Ithaca, NY 14853-2501.

¹S. C. Moss, D. T. Keating, and J. D. Axe, *Phase Transformations* (Pergamon, Oxford, 1973); D. T. Keating and S. J. LaPlaca, *J. Phys. Chem. Solids* **35**, 879 (1974).

²J. D. Axe, D. T. Keating, and S. C. Moss, *Phys. Rev. Lett.* **35**, 530 (1975).

³H. Wakabayashi, *Phys. Rev. B* **17**, 3875 (1978).

⁴Y. Nakagawa and A. D. B. Woods, in *Lattice dynamics*, edited by R. F. Wollis (Pergamon, Oxford, 1965).

⁵In the alloy $\text{Zr}_{0.8}\text{Nb}_{0.2}$ the diffuse neutron intensities are consistent with zero energy width; J. D. Axe, S. C. Moss, A. Heidemann, S. Howelles, and R. Pynn, *Solid State Commun.* **24**, 743 (1977).

⁶J. M. Rowe and A. Magerl, *Phys. Rev. B* **21**, 1706 (1980).

⁷H. Dosch and J. Peisl, *Phys. Rev. B* **32**, 623 (1985).

⁸R. Pynn (private communication); S. Shapiro and R. Pynn, *Bull. Am. Phys. Soc.* **23**, 313 (1978).

⁹S. C. Moss (private communication).

¹⁰B. S. Hickman, *J. Mater. Sci.* **4**, 554 (1969).

¹¹R. Currat and R. Pynn, in *Neutron Scattering in Material Science*, edited by G. Kostorz (Academic, New York, 1979).

¹²Y. A. Bagaryatskiy, G. I. Novosa, and T. V. Tagunova, *Dokl. Akad.* **24**, 743 (1955); *Dokl. Akad. Nauk SSSR* **105**, 1225 (1955).

¹³J. M. Silcox, M. H. Davies, and H. K. Hardy, *The Mechanism of Phase Transformation in Solids* (Institute of Metals, London, 1956).

¹⁴See Ref. 11 and references therein.

¹⁵C. W. Dawson and S. L. Sass, *Met. Trans.* **1**, 1225 (1970).

¹⁶R. Pynn, *J. Phys. F* **8**, 1 (1977).

¹⁷B. Borie, S. L. Sass, and A. Andreassen, *Acta Crystallogr. Sect. A* **29**, 585 (1973); **29**, 594 (1973).

¹⁸H. Kanzaki, *J. Phys. Chem. Solids* **2**, 107 (1957).

¹⁹E. Fromm and E. Gebhard, *Gase und Kohlenstoff in Metallen* (Springer, Berlin, 1976).

²⁰The total incoherent scattering from NbO_x is $S_{\text{inc}}(\mathbf{Q}) = se^{-2M}/4\pi + xs'e^{-2M'}/4\pi$, where s ($=0.27bn$), s' ($=0.04bn$) are the incoherent scattering power and $2M, 2M'$ the thermal Debye-Waller factors of Nb and O, respectively. From this we find that 2 at. % oxygen contributes less than 0.5% to the total incoherent scattering background and can, thus, be neglected.

²¹M. A. Krivoglaz, *Theory of X-Ray and Thermal Neutron Scattering by Real Crystals* (Plenum, New York, 1969).

²²H. Dosch, J. Peisl, and B. Dorner, *Z. Phys. B* (to be published).

²³This method for the conversion of the data into an absolute scale has important advantages compared to the common procedure which uses a Vanadium standard, as (i) the incident in-

tensity intercepted by the sample is precisely accounted for, (ii) multiple-scattering corrections do not have to be applied, and (iii) eventual uncertainties in the associated scattering lengths cancel out.

²⁴V. K. Tewary, *J. Phys. F* **3**, 1515 (1973).

²⁵H. Trinkaus, *Phys. Status Solidi B* **51**, 307 (1972).

²⁶P. H. Dederichs, *J. Phys. F* **3**, 471 (1973).

²⁷For a review of the location of interstitial defects in transition metals, see H. D. Carstanjen, habilitation thesis, University of Munich (1982).

²⁸P. Wombacher, doctoral thesis, Technische Hochschule Aachen, Federal Republic of Germany (1972); for an introduction to the properties of the force dipole tensor and its ex-

perimental determination see, e.g., H. Peisl, in *Hydrogen in Metals I*, Vol. 28 of *Topics in Applied Physics*, edited by G. Alefeld and J. Voelkl (Springer, Berlin, 1978).

²⁹H. Dosch, U. Schubert, H. Metzger, and J. Peisl, *J. Phys. F* **14**, 2467 (1984).

³⁰The concept of SRO is applied in this case to the rearrangement of the Nb atoms around one single oxygen impurity and must not be confused with a SRO of the impurities themselves. (Note that the defects under consideration are randomly distributed.)

³¹R. W. James, *The Optical Principles of the Diffraction of X-Rays* (Cornell University Press, Ithaca, New York, 1965).

³²C. B. Walker, *Phys. Rev. B* **28**, 674 (1983).